Effect of Filament Drawdown on Aerodynamic Drag and Heat Transfer in Fiber Spinning

C. Miller
3104 Loudoun Drive, Wilmington, DE 19808

DOI 10.1002/aic.10088
Published online in Wiley InterScience (www.interscience.wiley.com).

The momentum and thermal boundary layer equations are solved numerically to assess the effects of filament drawdown on aerodynamic drag and heat transfer in melt fiber spinning. It is found that, relative to the case without drawdown (constant filament velocity and diameter), the aerodynamic drag on the filament increases substantially, but the heat transfer rate is suppressed. Moreover, the air velocity profile eventually becomes fully developed (unlike the zero drawdown case), and the (velocity) boundary layer thickness, rather than continuing to grow with distance beneath the spinneret, eventually becomes proportional to the filament diameter, and thus decreases with increasing axial distance. Quantitative results are presented for the dimensionless drag force per unit length along the filament (the Drag number) and the Nusselt number as functions of the dimensionless axial distance and a new dimensionless parameter, the Drawdown Reynolds number. © 2004 American Institute of Chemical Engineers *AIChE J,* 50: 898–905, 2004
Keywords: fiber spinning, drawdown, air drag, heat transfer, boundary layer

Introduction

In the industrial unit operation of "melt fiber spinning" (a key step in the manufacture of man-made fibers), molten polymer filaments are extruded vertically downward through an array of capillaries (the "spinneret") and are extensionally drawn downward by a rotating roll (the "feed roll"), typically located 1–10 m beneath the spinneret, and rotating at a linear speed on the order of 100 × the nominal "jet" velocity of the polymer exiting the capillary (Figure 1). During their relatively short time of travel between the spinneret and feed roll (typically 0.1–3 s), the polymeric filaments experience significant thermal and aerodynamic drag interactions with the surrounding air. These interactions can play a substantial role in influencing both product properties and process operability.

The filaments cool on the order of 200°C along the spinline, and their tensions (and associated tensile stress) increase significantly, in large part the result of aerodynamic drag (in addition to inertial acceleration). This combination of temperature history and stress history for the polymer uniquely determines the detailed axial variations of polymer deformation, crystallization, and molecular orientation, and thereby ultimately determines the mechanical properties (such as elongation to break, tenacity) of the as-spun filaments.

From the standpoint of process operability, the filament temperature at the feed roll must be reduced sufficiently to prevent the filament from sticking to the roll. Furthermore, any molecular orientation developed between the spinneret and the feed roll can limit the extent of additional fiber property development achievable in subsequent (and more orientationally efficient) mechanical draw steps, without incurring filament breakage.

In practice, the interactions between the spinning filaments and the surrounding air can often be extremely difficult to quantify accurately. Some of the complexities involved include:

• *Interactions between filament boundary layers within a multifilament array.* In the absence of imposed cross flow, the boundary layers on the filaments of a multifilament array grow very rapidly with distance from the spinneret, and soon begin to impinge upon one another. This tends to reduce both the drag and heat transfer rates on the individual filaments (on average), relative to the case of an isolated spinning filament (Matsui, 1976). It also tends to produce variations with lateral position in the array as a result of horizontal cross flow induced

C. Miller's e-mail address is ChesterMiller@Mindspring.com.

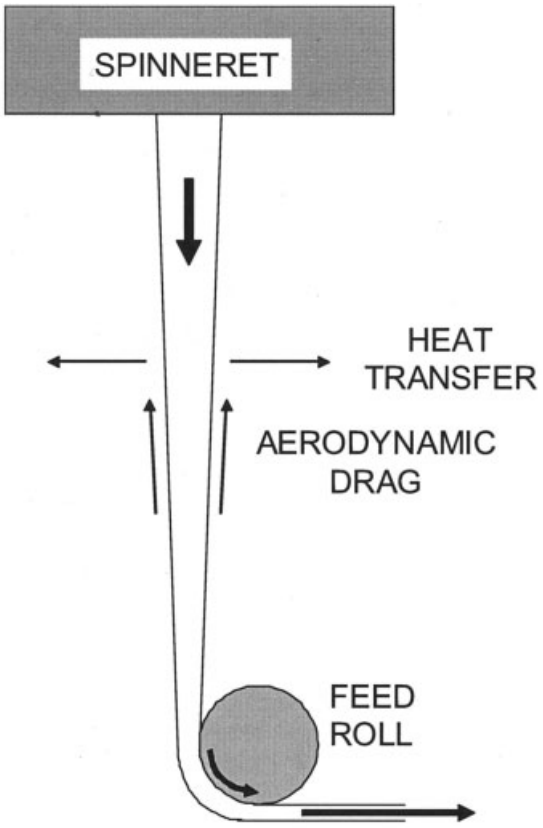

Figure 1. Fiber spinning operation.

by the air entrainment demands of the filaments closer to the center of the array. Deliberately imposed cross flow can add to this variability.

- *Turbulent flow.* The boundary layers on the filaments are expected to be laminar in the region closer to the spinneret (typically <1 m), and to transition to turbulence further toward the feed roll. Furthermore, in the case of a multifilament array, the transition can occur even sooner, and the turbulence intensity can be greater, if the entrainment pumping requirements of the array are not fully satisfied by a separate, deliberately imposed, supply of air blown into or across the array.

- *Cross flow.* Cross-flow air is also often deliberately introduced over the initial portion of the spinline to enhance the quenching rate, control property development, and shorten the overall length of the unit. Irrespective of whether it is imposed deliberately or whether it is the result of array air entrainment, cross flow exerts a very significant impact on both the heat transfer and the drag. It is surprising that, until only recently, the effect of cross flow on axial drag had not been recognized nor incorporated into spinning models (see Beyreuther and Brünig, 1997; Brünig, et al., 1999). Even a cursory inspection of the differential momentum and energy balance equations with cross flow present reveals that, for the ideal limiting case of constant filament velocity, the heat transfer rate is identical to that for flow over a stationary cylinder, and the axial drag can be deduced directly from the heat transfer relation by applying Reynolds analogy (at least in the laminar flow region). Moreover, with just a modest cross-flow velocity present, the axial growth of the momentum and thermal boundary layers (which is known to take place in the total absence of cross flow; see below) entirely ceases (that is, the boundary layers become fully developed), and resumes only after the filaments have emerged from the imposed cross-flow region. For axial locations beyond the onset of turbulence, Kase and Matsuo (1967) developed a relationship for combining the contributions of cross flow and axial flow to the overall heat transfer, and Beyreuther and Brunig (1997) did the same for the axial drag. However, in the limit of zero cross-flow velocity, the Kase–Matsuo relationship significantly exceeds the heat transfer rate one would deduce from Matsui's axial drag correlation using Reynolds analogy (Denn, 1996). Denn recommended a modification for use in spinning models.

- *Filament drawdown.* As a spinning filament deforms extensionally within the region between the spinneret and the feed roll, its velocity increases and its diameter correspondingly decreases. This effect is referred to as filament drawdown. The increasing filament velocity forces the adjacent "entrained" air to likewise accelerate, which increases the drag on the filament. Moreover, the change in the radial velocity profile within the velocity boundary layer also has an impact on the filament heat transfer. To date, the effects of filament drawdown have not been systematically analyzed in terms of the fundamental heat and momentum transfer behavior, nor have they been accounted for in any state-of-the-art fiber-spinning models.

In practice, these uncertainties can be comparable to other large uncertainties encountered in modeling the spinning operation, such as those associated with the rheological and/or crystallization behavior of the polymer. It would appear that there is a need for significant additional fundamental fluid mechanics and heat-transfer studies to be carried out, to more accurately quantify the interactions between the spinning filaments and the surrounding air. As an initial step in that direction, the present work focuses on the effect of filament drawdown on axial drag and heat transfer on a single isolated spinline in the laminar flow region, in the absence of cross flow. Although this set of boundary conditions deviates substantially from the norm in actual spinning practice, it is often encountered in bench-scale studies to develop basic data for a spinning operation or to obtain a better understanding of an existing system. Moreover, from a mechanistic point of view, it can provide a qualitative picture of the effects of drawdown in the turbulent flow region.

Initial fundamental studies of filament drag and heat transfer in fiber spinning were carried out by Sakiadis (1961b; drag) and Bourne and Elliston (1970; heat transfer). These studies considered the ideal limiting case of constant filament velocity (no drawdown) and laminar flow, and found that, immediately after the filaments emerge from the spinneret, air boundary layers begin to develop on the filaments; moreover, these boundary layers grow without limit as a function of distance beneath the spinneret (until the flow transitions to turbulence). Using the Karman–Pohlhausen integral method, they developed approximate solutions to the momentum and energy boundary layer equations, to obtain the drag coefficient and Nusselt number as a function of the dimensionless axial distance (and Prantdl number, in the case of heat transfer). Because of the increasing boundary layer thicknesses, the drag coefficient and Nusselt number were found to decrease monotonically with increasing distance.

The only literature studies to briefly touch on the quantitative effects of filament drawdown on drag and heat transfer in fiber spinning were those of Sayles and Caswell (1984) and Kubo (1991). Sayles and Caswell developed a spinning model for the region close to the spinneret, approximating the air drag using the Karman–Pohlhausen integral technique, and then invoking Reynolds analogy to estimate the heat transfer. Their drag analysis and calculated results are consistent with those of the present study, in that the drag increased with drawdown present. However, their use of Reynolds analogy to estimate the heat transfer is not supported by the current findings, which demonstrate that, when drawdown is occurring, the Reynolds analogy is invalid and heat transfer is suppressed rather than enhanced. Kubo examined a specific set of spinning conditions (rather than carrying out a more systematic assessment of the drawdown effect), likewise using the integral technique. In agreement with the present (more general) evaluation, he found that, unlike the case of constant filament velocity (where the boundary layer grows without bound), with filament drawdown present, the velocity profile within the boundary layer becomes fully developed, and its thickness actually *decreases* with axial distance from the spinneret, rapidly becoming directly proportional to the local filament diameter.

The present development attacks the problem of filament drawdown in a more systematic and general fashion, by reducing the momentum and thermal boundary layer equations to dimensionless form, and then solving numerically for the dimensionless drag and heat-transfer coefficients as a function of the dimensionless distance beneath the spinneret, and a new characteristic dimensionless group, the Drawdown Reynolds number.

Problem Formulation

For a spinning filament that is experiencing drawdown, the filament axial velocity $V(z)$ and radius $a(z)$ are related to one another by the overall mass balance equation

$$V(z)a^2(z) = \frac{M}{\rho\pi} = \text{Constant} \tag{1}$$

where M is the mass rate of flow per capillary and ρ is the polymer density (assumed approximately constant).

In the air surrounding the filament, the flow and heat transfer are governed by the continuity equation, and the axial momentum balance and energy balance boundary layer equations (Bourne and Elliston, 1970)

$$\frac{1}{r}\frac{\partial(ur)}{\partial r} + \frac{\partial w}{\partial z} = 0 \tag{2}$$

$$ur\frac{\partial w}{\partial r} + wr\frac{\partial w}{\partial z} = \nu\frac{\partial}{\partial r}\left(r\frac{\partial w}{\partial r}\right) \tag{3}$$

$$ur\frac{\partial T}{\partial r} + wr\frac{\partial T}{\partial z} = \alpha\frac{\partial}{\partial r}\left(r\frac{\partial T}{\partial r}\right) \tag{4}$$

where u is the radial velocity, w is the axial velocity, T is the temperature, and ν and α are the kinematic viscosity and thermal diffusivity of the air, respectively (treated as constant in the present development).

Boundary conditions on the flow and heat transfer are as follows

$$w = V(z) \quad \text{at} \quad r = a(z) \tag{5a}$$

$$w \to 0 \quad \text{at} \quad r \to \infty \tag{5b}$$

$$w = 0 \quad \text{at} \quad z = 0 \tag{5c}$$

$$u = V\frac{da}{dz} \quad \text{at} \quad r = a(z) \tag{5d}$$

$$T = T_\infty \quad \text{at} \quad z = 0 \tag{5e}$$

$$T = T_S(z) \quad \text{at} \quad r = a(z) \tag{5f}$$

$$T \to T_\infty \quad \text{at} \quad r \to \infty \tag{5g}$$

Henceforth, it will be assumed that the temperature at the surface of the filament T_S is a constant. Although in actual fiber spinning, this is typically not the case (the fiber temperature usually cools substantially along the spinline), the present results provide an important upper bound to the heat-transfer rate. Moreover, the conclusions from the present study regarding the qualitative effect of filament drawdown on heat transfer would not be expected to change if filament cooling were included.

Integrating the continuity equation (Eq. 2) radially from the surface of the filament to any arbitrary radial position (subject to boundary conditions Eq. 5d and Eq. 1) yields

$$ur = -\frac{1}{2}\frac{\partial}{\partial z}\int_{a^2}^{r^2} w\,d(r^{*2}) \tag{6}$$

where the asterisk (*) denotes a dummy variable of integration, and where, in deriving Eq. 6, use has been made of the Leibnitz formula for differentiation under the integral sign.

Substitution of Eq. 6 into Eqs. 3 and 4 eliminates the radial velocity u from the analysis and gives the following

$$-\frac{1}{2}\left[\frac{\partial}{\partial z}\int_{a^2}^{r^2} w\,d(r^{*2})\right]\frac{\partial w}{\partial r} + wr\frac{\partial w}{\partial z} = \nu\frac{\partial}{\partial r}\left(r\frac{\partial w}{\partial r}\right) \tag{7a}$$

$$-\frac{1}{2}\left[\frac{\partial}{\partial z}\int_{a^2}^{r^2} w\,d(r^{*2})\right]\frac{\partial T}{\partial r} + wr\frac{\partial T}{\partial z} = \alpha\frac{\partial}{\partial r}\left(r\frac{\partial T}{\partial r}\right) \tag{7b}$$

We next introduce the following set of dimensionless parameters and coordinate transformations

$$\phi = \ln\left(\frac{r}{a(z)}\right)^2 \tag{8a}$$

$$\xi = \frac{4\nu z}{Va^2} \tag{8b}$$

$$f(\xi, \phi) = \frac{w}{V(z)} \tag{8c}$$

$$g(\xi, \phi) = \frac{T - T_\infty}{(T_S - T_\infty)} \tag{8d}$$

Equation 8a maps the axially varying radial filament boundary location onto the line $\phi = 0$. This greatly simplifies the subsequent numerical solution of the equations.

Substitution of Eqs. 8a–8d into Eqs. 7a and 7b, and into boundary conditions Eqs. 5a–5g, yields the following

$$f\frac{\partial f}{\partial \xi} - \frac{\partial f}{\partial \phi}\frac{\partial}{\partial \xi}\left[\int_0^\phi e^{-(\phi-\phi^*)} f(\xi, \phi^*) d\phi^*\right] + \mathrm{Re}\, f^2 = e^{-\phi}\frac{\partial^2 f}{\partial \phi^2} \tag{9a}$$

$$f\frac{\partial g}{\partial \xi} - \frac{\partial g}{\partial \phi}\frac{\partial}{\partial \xi}\left[\int_0^\phi e^{-(\phi-\phi^*)} f(\xi, \phi^*) d\phi^*\right] = \frac{1}{\mathrm{Pr}} e^{-\phi}\frac{\partial^2 g}{\partial \phi^2} \tag{9b}$$

$$f = 1 \quad \text{at} \quad \phi = 0 \tag{10a}$$

$$f \to 0 \quad \text{at} \quad \phi \to \infty \tag{10b}$$

$$f = 0 \quad \text{at} \quad \xi = 0 \quad (\phi > 0) \tag{10c}$$

$$g = 1 \quad \text{at} \quad \phi = 0 \tag{10d}$$

$$g \to 0 \quad \text{at} \quad \phi \to \infty \tag{10e}$$

$$g = 0 \quad \text{at} \quad \xi = 0 \quad (\phi > 0) \tag{10f}$$

where Pr is the Prantdl number, and where $\mathrm{Re} = \mathrm{Re}(\xi)$ is an entirely new parameter that has emerged automatically from the present analysis, uniquely capturing the effects of filament drawdown. We henceforth refer to this parameter as the (local) Drawdown Reynolds number, defined according to the following equation

$$\mathrm{Re}(\xi) = \frac{Va^2}{4\nu}\frac{d \ln V(z)}{dz} = \frac{d \ln V(\xi)}{d\xi} \tag{11}$$

Previous theoretical and experimental analyses of heat transfer and drag in fiber spinning have failed to recognize the Drawdown Reynolds number as a significant parameter.

In general, the Drawdown Reynolds number will be a function of the dimensionless axial coordinate ξ, in which case one would conclude that a fully developed solution to Eq. 9a (in the sense that the solution is independent of ξ and dependent only on the dimensionless radial coordinate ϕ), would not generally exist. However, if the filament axial velocity $V(z)$ varies in such a way that $(d \ln V)/dz$ is a constant along the spinline, then the Drawdown Reynolds number Re will also be essentially constant, and a fully developed solution will exist. This fully developed solution is of significant practical interest for a number of reasons. First, in the limit of isothermal spinning of a Newtonian fluid with negligible inertia and drag, $(d \ln V)/dz$ is exactly constant over the entire spinline. Furthermore, in practice, $(d \ln V)/dz$ is often found to vary very slowly over large segments of the spinline, and the fully developed solution may provide a very accurate local approximation to the exact solution. The validity of this approximation will depend on the axial length scale for Re variation compared to the axial length scale for development of the fully developed velocity profile. Note, from the definition of the parameter ϕ (Eq. 8a), that the thickness of the fully developed boundary layer will be directly proportional to the local filament radius $a(z)$.

Comparison of Eq. 16a for gas velocity and 16b for gas temperature reveals that, as a consequence of the presence of the drawdown/acceleration term in the momentum equation, the two relationships are not analogous mathematically. This implies that the Reynolds analogy between heat and momentum transfer will not, in general, apply with drawdown present. (The analogy would be preserved only if the temperature driving force between the filament surface and the far-field gas were *increasing* in magnitude with distance along the spinline at a rate equivalent to the rate of increase of the velocity driving force. However, this is essentially the opposite of the situation typically encountered in practice with melt spinning, where the temperature driving force *decreases* with distance from the spinneret.)

The drag force per unit length F and the heat transfer rate per unit length Q on the filament are given, respectively, by the following equations

$$F = -2\pi a\mu\left(\frac{\partial w}{\partial r}\right)_{r=a} \tag{12a}$$

$$Q = -2\pi ak\left(\frac{\partial T}{\partial r}\right)_{r=a} \tag{12b}$$

where μ is the gas viscosity and k is the thermal conductivity. If we substitute Eq. 8a into these relationships we obtain

$$\frac{F}{\pi\mu V} = \mathrm{Dr} = -4\left(\frac{\partial f}{\partial \phi}\right)_{\phi=0} \tag{13a}$$

$$\frac{Q}{\pi k(T_S - T_\infty)} = \mathrm{Nu} = -4\left(\frac{\partial g}{\partial \phi}\right)_{\phi=0} \tag{13b}$$

where Nu is the dimensionless Nusselt number for heat transfer and Dr is the analogous "Drag number." Although, for most applications involving aerodynamic drag on a body, the dimensionless drag coefficient C_D is the parameter most frequently used in the literature, in the case of fiber spinning, the dimensionless drag number (as defined above) is more convenient to work with because of its analogous form to the Nusselt number, as well as its direct relationship to the filament tension gradient (for application in spinning models). The conventional

drag coefficient C_D is related to the Drag number by the equation

$$C_D = \mathrm{Dr}\left(\frac{\nu}{Va}\right) \tag{14}$$

This completes the problem formulation.

Solution to Model Equations

Solution in limit of small ξ

At very small values of ξ, the size of the velocity and temperature boundary layers will be small compared to the radius of the filament and, thus, the solution will essentially reduce to that for an infinitely wide flat sheet emerging from a slot in a wall into an semi-infinite domain. In Eqs. 9a and 9b, the exponential terms involving ϕ will approach unity within the boundary layers, and the "feedback sink" provided by the Drawdown Reynolds number term in Eq. 9a will be negligible compared to the other terms in the relationship, thus giving

$$f\frac{\partial f}{\partial \xi} - \frac{\partial f}{\partial \phi}\frac{\partial}{\partial \xi}\left[\int_0^{\phi} f(\xi, \phi^*)d\phi^*\right] = \frac{\partial^2 f}{\partial \phi^2} \tag{16a}$$

$$f\frac{\partial g}{\partial \xi} - \frac{\partial g}{\partial \phi}\frac{\partial}{\partial \xi}\left[\int_0^{\phi} f(\xi, \phi^*)d\phi^*\right] = \frac{1}{\mathrm{Pr}}\frac{\partial^2 g}{\partial \phi^2} \tag{16b}$$

According to Eqs. 16a and 16b, Reynolds analogy between drag and heat transfer is recovered in the limit of small ξ, in the sense that, at Pr = 1, the solution for the dimensionless temperature g will be identical to the solution for the dimensionless velocity f.

Sakiadis (1961a) and Shih and Middleman (1970) applied a similarity transformation to convert Eqs. 16a and 16b from partial differential equations (PDEs) to ordinary differential equations (ODEs), and then integrated the resulting ODEs numerically to obtain the dimensionless velocity and temperature profiles, as well as the dimensionless drag and heat transfer parameters. In terms of the Drag number and Nusselt number, their results can be summarized as follows

$$\mathrm{Dr} = \frac{1.775}{\sqrt{\xi}} \tag{17}$$

and

$$\mathrm{Nu} = \frac{1.775}{\sqrt{\xi}}\beta(\mathrm{Pr}) \tag{18}$$

where, in the vicinity of Pr = 1 (gases), the function β is very closely approximated by

$$\beta(\mathrm{Pr}) \cong \mathrm{Pr}^{2/3} \tag{19}$$

If we substitute Eq. 19 into Eq. 18, we obtain

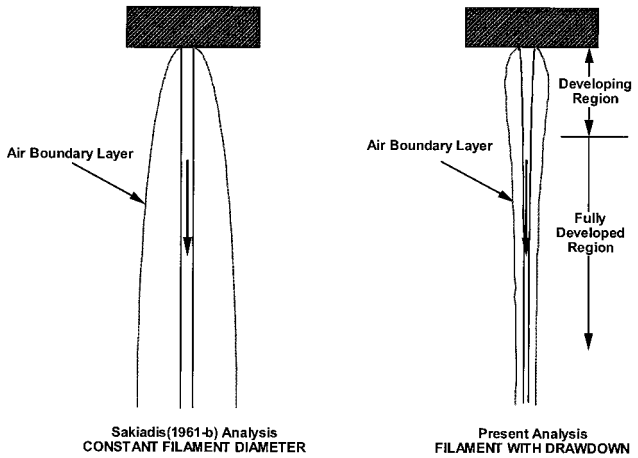

Figure 2. Comparison of velocity boundary layer thickness variations with and without drawdown.

$$\mathrm{Nu} = \frac{1.775}{\sqrt{\dfrac{\xi}{\mathrm{Pr}^{4/3}}}} \tag{20}$$

According to Eqs. 17 and 20, in the vicinity of Pr = 1 (Pr = 0.7 to 1.0), the Nusselt number expressed as a function of $\xi/\mathrm{Pr}^{4/3}$ is essentially identical to the Drag number expressed as a function of ξ. We will show below that exactly the same Prantdl number "shift factor" accurately applies not only for small ξ, but over the full range of ξ values, provided the Drawdown Reynolds number is zero (that is, no drawdown).

Solution in limit of large ξ (Re > 0)

At very large values of ξ, we find that the velocity profile becomes fully developed in terms of the dimensionless radial coordinate ϕ, whereas the temperature profile continues to change with ξ. The boundary layer equations for momentum and heat transfer (Eqs. 9a and 9b) reduce, in this region, to

$$\mathrm{Re}\, f^2 = e^{-\phi} f'' \tag{21a}$$

$$f(\phi)\frac{\partial g}{\partial(\xi/\mathrm{Pr})} = e^{-\phi}\frac{\partial^2 g}{\partial \phi^2} \tag{21b}$$

A velocity profile that depends only on ϕ implies that, within the fully developed region, the velocity boundary layer thickness, rather than continuing to grow with distance beneath the spinneret, eventually becomes proportional to the filament diameter, and thus decreases with increasing axial distance. A comparison between results reported by Sakiadis (1961b) for constant filament diameter (without drawdown) and the present results for velocity boundary layer development with drawdown is illustrated schematically in Figure 2.

Because the dimensionless velocity is not a function of ξ, the Prantdl number effect in the thermal boundary layer equation has been absorbed directly into the dimensionless axial distance parameter, such that, at a given value of Re, the dimensionless temperature is a function of only ξ/Pr and ϕ (but not Pr separately).

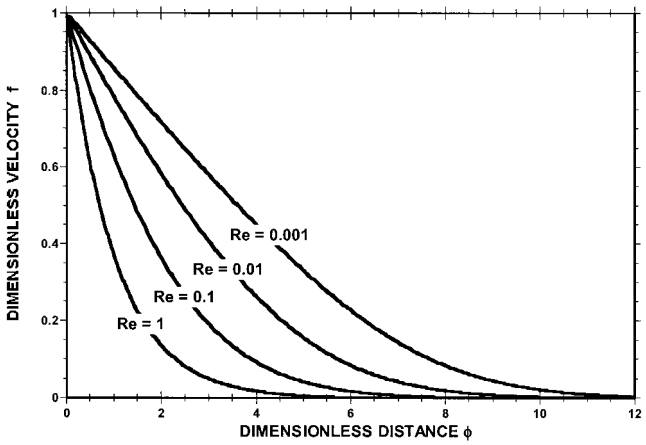

Figure 3. Fully developed velocity profiles with drawdown present.

In this section, we solve Eq. 21a numerically, subject to boundary conditions 10a and 10b, for the fully developed velocity profile at a selection of values for the Drawdown Reynolds number Re. We also present results for the dimensionless Drag number as a unique function of the Drawdown Reynolds number, applicable throughout the fully developed region.

Before proceeding with the numerical solution to Eqs. 21a and 21b, however, we note first that, for the special case of Re = 1, an analytic solution exists. This analytic solution is used in the subsequent development to verify the results of our numerical calculations. The analytic solution for Re = 1 is given by

$$f = e^{-\phi} \qquad (\mathrm{Re} = 1) \tag{22a}$$

or, equivalently

$$w = \frac{Va^2}{r^2} \qquad (\mathrm{Re} = 1) \tag{22b}$$

and

$$g = \mathrm{erfc}\left(\frac{\phi}{2\sqrt{\xi/\mathrm{Pr}}}\right) \qquad (\mathrm{Re} = 1) \tag{22c}$$

where erfc is the complementary error function. If we substitute Eqs. 22a–22c into Eqs. 13a and 13b for the Drag number and Nusselt number, we obtain

$$\mathrm{Dr} = 4 \qquad \text{at} \qquad \mathrm{Re} = 1 \tag{23a}$$

$$\mathrm{Nu} = \frac{4}{\sqrt{\pi\xi/\mathrm{Pr}}} = \frac{2.26}{\sqrt{\xi/\mathrm{Pr}}} \qquad \text{at} \qquad \mathrm{Re} = 1 \tag{23b}$$

Let us now consider the numerical solution of Eq. 21a, subject to boundary conditions 10a and 10b, for the fully developed velocity profile at arbitrary drawdown Reynolds number. These equations constitute a split boundary value problem, which has been solved in the present development using the "shooting method." This involved assuming an initial value for $f'(\phi)$ at $\phi = 0$, and then integrating the differential equation from $\phi = 0$ to very large ϕ (in this case $\phi = 20$) as an initial value problem; the initial guess was iterated upon until convergence was achieved on boundary condition 10b at the far boundary. The numerical integrations were carried out using the highly accurate and widely used automatic double-precision ODE integration package DVODE, which is freeware available over the Internet.

Figure 3 shows the calculated fully developed velocity profiles at a selection of values for the Drawdown Reynolds number Re ranging from 0.001 to 1 (which are illustrative of values typically encountered in practice). As the Drawdown Reynolds number decreases in magnitude, the velocity boundary layer thickness increases. For the case of Re = 1, the largest Re shown, the "1%" boundary layer thickness is equal to $\phi = 4.6$, which, from Eq. 8a, translates into a radial distance equal to five filament diameters. The corresponding "1%" boundary layer thicknesses for Re = 0.001, Re = 0.01, and Re = 0.1 are 122, 41, and 14 filament diameters, respectively. For typical filament dimensions encountered in practice, some of these boundary layer thicknesses can easily exceed the distance between filaments in a multifilament array, and in some cases, can even approach the lateral dimensions of the quench unit.

Figure 4 shows the calculated Drag number plotted as a function of the Drawdown Reynolds number (the plotted points represent the results from the numerical calculations). As will be observed, the Drag number increases monotonically with increasing Re. The curve plotted in the figure provides an excellent analytic fit to the numerical results over the full range of Re considered, and is given by

$$\mathrm{Dr} = 4\,\mathrm{Re}^{[0.418+0.02\,\ln(\mathrm{Re})]} \qquad (0.001 < \mathrm{Re} < 1) \tag{24}$$

The numerical solution at Re = 1 was found to agree with the analytic result (Dr = 4) to at least four significant figures.

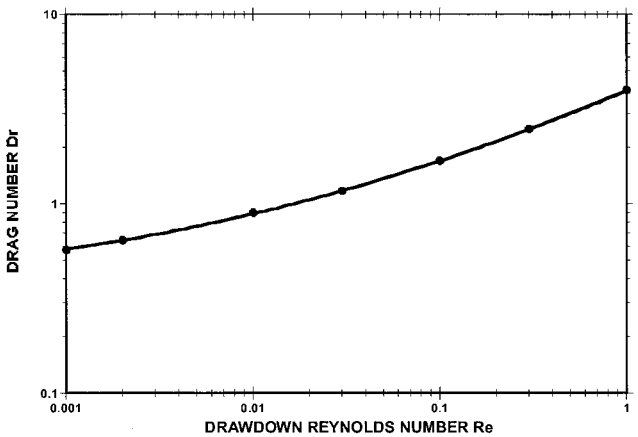

Figure 4. Drag number as a function of Drawdown Reynolds number for fully developed region (plotted points represent results from present numerical calculations).

This verifies the high degree of accuracy of the current numerical solution procedure.

Solution for arbitrary ξ

In the present development, the numerical solution to the dimensionless drag and thermal boundary layer equations (Eqs. 9a and 9b) was obtained using the "method of lines." Here, the PDEs were discretized with respect to the dimensionless radial coordinate ϕ using second-order finite-difference approximations, and the resulting set of ODEs in ξ were integrated numerically as an initial value problem using the stiff ODE option of the DVODE integration package. Because of a minor singularity in the PDEs at $\xi = 0$ (where the dimensionless velocity f is equal to zero at all $\phi > 0$), the numerical integration was actually initiated at a small finite value of ξ ($\xi = 0.005$), using the limiting solution for small ξ (see above) as an initial condition.

The results of the numerical calculations for the case of Re = 0 (no drawdown) are shown in Figure 5, in which the Drag number is plotted as a function of ξ, and the Nusselt number is plotted as a function of $\xi/\mathrm{Pr}^{4/3}$ (for the specific case of Pr = 0.7). As will be observed, the two curves superimpose almost perfectly over the full range of ξ (of course, for the case of Pr = 1, they would superimpose exactly). This implies the existence of a Reynolds-type analogy of the form

$$\mathrm{Nu}(\xi, \mathrm{Pr}) \approx \mathrm{Dr}\left(\frac{\xi}{\mathrm{Pr}^{2/3}}\right) \qquad (0.7 < \mathrm{Pr} < 1.0) \qquad (25)$$

in the limit of zero Drawdown Reynolds number. Also shown in Figure 5 are the results of Bourne and Elliston (1970) for Dr, and for Nu at Pr = 0.72 (again plotted in terms of ξ and $\xi/\mathrm{Pr}^{4/3}$, respectively), which were obtained using the Karman–Pohlhausen approximate method. Their findings are somewhat lower than the present more accurate values, calculated using numerical integration. Based on a comparison with the numerical calculations of Glauert and Lighthill (1955) for the case of axial flow over a fixed cylinder, Bourne and Elliston suggested a set of correction factors (as a function of ξ) to compensate for

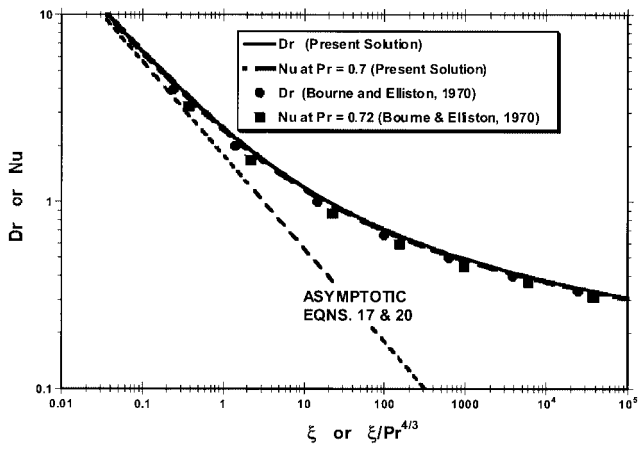

Figure 5. Calculated Drag and Nusselt numbers in the absence of drawdown (Re = 0): Dr plotted vs. ξ and Nu plotted vs. $\xi/\mathrm{Pr}^{4/3}$.

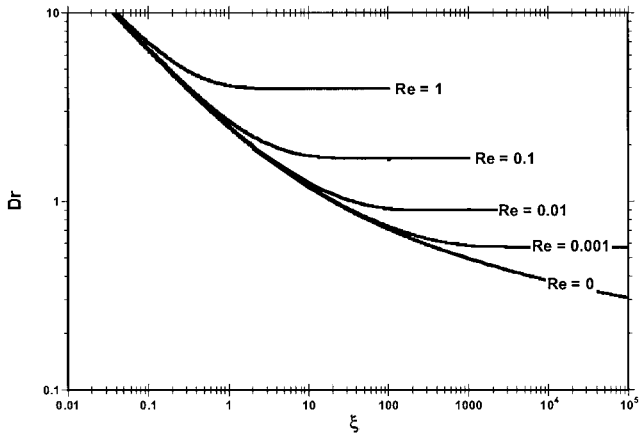

Figure 6. Effect of filament drawdown on aerodynamic drag.

the small inaccuracy associated with the Karman–Pohlhausen method. If we had applied these correction factors the Bourne and Elliston results in Figure 5, their plotted points would have fallen directly on the curve representing the present numerical findings. In terms of the current parameters, Bourne and Elliston's results for Dr and Nu again appear to fall on a single curve, consistent with the Reynolds-type analogy expressed by Eq. 25.

The results for Re = 0 were very accurately fit over the full range of values of ξ considered in Figure 5 ($0.005 < \xi < 10^5$) by the equation

$$\mathrm{Dr}(\xi) = \frac{2.5053}{\xi^{0.36316 - 0.018395 \ln \xi - 0.00045107(\ln \xi)^2 + 6.0398x10^{-5}(\ln \xi)^3}} \qquad (26)$$

Figure 6 shows the calculated effect of filament drawdown on the aerodynamic drag. With drawdown present (Re > 0), the filament drag is always found to be greater than that in the absence of drawdown (Re = 0). At values of $\xi < 0.1/\mathrm{Re}$, the Drag number for all Re > 0 is only slightly higher than that with Re = 0. At values of $\xi > 3/\mathrm{Re}$, the Drag number has leveled off at a constant value, representative of the result for the fully developed region. In the span between $\xi = 0.1/\mathrm{Re}$ and $\xi = 3/\mathrm{Re}$, the Drag number undergoes a relatively rapid transition between the behavior for small ξ and the fully developed constant value at large ξ.

As an indication of accuracy of the present "method of lines" spatial finite-difference solution to the PDEs, the calculated fully developed Drag numbers have been compared with the values obtained in the previous section using the inherently more accurate "shooting method." The values obtained in the current development by both methods differed from one another by less than 0.1% for all Re considered (over the range of $\Delta\phi$ values used in the current method of lines finite difference discretizations).

As indicated previously, even if the Drawdown Reynolds number is not constant with ξ, the current results for the fully developed region might nonetheless provide an accurate estimate of the Drag number, provided the length scale for the Drawdown Reynolds number variation is large compared to the length scale for development of the fully developed solution.

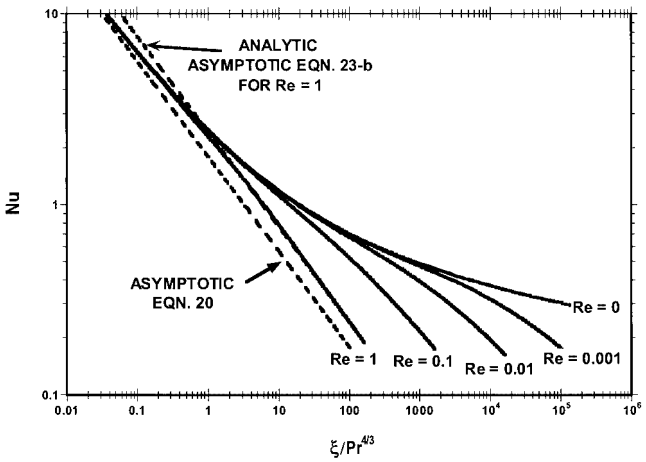

Figure 7. Effect of filament drawdown on heat transfer (Pr = 0.7).

Based on the results in Figure 6, this can now be roughly quantified. The dimensionless length scale for the Drawdown Reynolds number variation is on the order of $|[d\ \ln(\mathrm{Re})]/d\xi|^{-1}$, whereas the dimensionless length scale for development of the fully developed solution is on the order of 3/Re. Therefore, for this estimation procedure to be valid, we must have that

$$\left|\frac{d\ \ln(\mathrm{Re})}{d\xi}\right| \ll \frac{\mathrm{Re}}{3} \tag{27a}$$

or equivalently, that

$$\left|\frac{d(1/\mathrm{Re})}{d\xi}\right| \ll \frac{1}{3} \tag{27b}$$

Figure 7 shows the calculated effect of filament drawdown on heat transfer for the specific case of Pr = 0.7 (air). With drawdown present (Re > 0), the heat transfer is always found to be suppressed relative to the case without drawdown (Re = 0). At values of $\xi < 1/\mathrm{Re}$, the Nusselt number is only slightly lower than that with Re = 0. However, as ξ increases further, the curves for Re > 0 are found to depart substantially downward from the curve for Re = 0. Also shown in Figure 7 is the analytic asymptote for the Re = 1 curve, which applies in the limit of large ξ (Eq. 23b). The current numerical solution very closely approaches this asymptote at values of $\xi > 2$.

The fundamental cause of the decrease in the heat transfer rate when drawdown is present is related to the formation of the fully developed velocity profile. Once the fully developed profile has set in, its shape remains fixed in terms of the dimensionless radial parameter ϕ, whereas the thermal boundary layer continues to grow. Moreover, the fully developed velocity profile drops off much more rapidly with ϕ than in the case without drawdown. Therefore, the thermal boundary layer soon begins growing radially into a region of very low axial velocities. This tends to trap the heat near the filament, causing the thermal boundary layer to grow much more rapidly, and thus stifling the heat-transfer rate.

Summary and Conclusions

In the present development, the effects of filament drawdown on aerodynamic drag and heat transfer in melt fiber spinning have been assessed. It has been found that, relative to the case without drawdown, the aerodynamic drag increases substantially, but the heat-transfer rate is suppressed. The Drag number (characterizing aerodynamic drag) and the Nusselt number (characterizing heat transfer) have been quantified in terms of a new parameter, the Drawdown Reynolds number. It has also been shown that, when drawdown is present, the velocity boundary layer on the filament becomes fully developed, and its thickness becomes proportional to the filament diameter. This departs significantly from the behavior that exists in the absence of drawdown. Finally, for the case without drawdown, it has been found that a special form of Reynolds-type analogy exists between heat transfer and drag that applies over the full range of Prantdl numbers characteristic of gases (0.7–1.0).

The present results apply strictly to the region of laminar flow, within approximately 1 m from the spinneret. However, for the turbulent flow region further downstream, we can expect a similar type of mechanistic behavior to occur, although possibly to a lesser extent.

In practice, the uncertainties and complexities associated with the interaction between the spinning filaments and the surrounding air are extensive, and the present development is only a first step in narrowing the uncertainties. In the author's judgment, much additional fundamental work needs to be done.

Literature Cited

Beyreuther, R., and H. Brünig, "High Filament Velocities in the Underpressure Spunbonding Nonwoven Process," *Int. Fiber J.*, **Dec**., 129 (1997).

Bourne, D. E., and D. G. Elliston, "Heat Transfer Through the Axially Symmetric Boundary Layer on a Moving Circular Fibre," *Int. J. Heat Mass Transfer*, **13**, 583 (1970).

Brünig, H., R. Beyreuther, and H. Hofman, "The Influence of Quench Air on Fiber Formation and Properties in the Melt Spinning Process," *Int. Fiber J.*, **Apr**., 104 (1997).

Denn, M. M., "Correlations for Transport Coefficients in Textile Fiber Spinning," *Ind. Eng. Chem. Res.*, **35**, 2842 (1996).

Glauert, M. B., and M. J. Lighthill, "The Axisymmetric Boundary Layer on a Long Thin Cylinder," *Proc. R. Soc. Lond. A Phys. Sci.*, **A230**, 188 (1955).

Kase, S., and T. Matsuo, "Studies on Melt Spinning. II. Steady-State and Transient Solutions of Fundamental Equations Compared With Experimental Results," *J. Appl. Polym. Sci.*, **11**, 251 (1967).

Kubo, S., "Air Boundary Layer on a Filament in High-Speed Spinning," in *High-Speed Fiber Spinning—Science and Engineering Aspects*, A. Ziabicki, and H. Kawai, eds., Krieger, Malabar, FL, p. 115 (1991).

Matsui, M., "Air Drag on a continuous Filament in Melt Spinning," *Trans. Soc. Rheol.*, **20**, 465 (1976).

Sakiadis, B. C., "Boundary-Layer Behavior on Continuous Solid Surfaces: II. The Boundary Layer on a Continuous Flat Surface," *AIChE J.*, **7**, 221 (1961a).

Sakiadis, B. C., "Boundary-Layer Behavior on Continuous Solid Surfaces: III. The Boundary Layer on a Continuous Cylindrical Surface," *AIChE J.*, **7**, 467 (1961b).

Sayles, R. E., and B. Caswell, "A Finite-Element Analysis of the Upper Jet Region of a Fiber Drawing Flow Field of a Temperature-Sensitive Material," *Int. J. Heat Mass Transfer*, **27**, 57 (1984).

Manuscript received Mar. 8, 2003, and revision received Aug. 11, 2003.